◆ Human Brain Mapping 37:1903–1919 (2016) ◆

Combining Tract- and Atlas-Based Analysis Reveals Microstructural Abnormalities in Early Tourette Syndrome Children

Hongwei Wen,[1,2] Yue Liu,[3,4] Jieqiong Wang,[1] Islem Rekik,[5] Jishui Zhang,[3,4] Yue Zhang,[3,4] Hongwei Tian,[3,4] Yun Peng,[3,4]* and Huiguang He[1,2]*

[1]State Key Laboratory of Management and Control for Complex Systems, Institute of Automation, Chinese Academy of Sciences, Beijing, China
[2]Research Center for Brain-Inspired Intelligence, Institute of Automation, Chinese Academy of Sciences, Beijing, China
[3]Department of Radiology, Beijing Children's Hospital, Capital Medical University, Beijing, China
[4]Beijing Key Lab of Magnetic Imaging Device and Technique, Beijing Children's Hospital, Capital Medical University, Beijing, China
[5]Department of Radiology and BRIC, University of North Carolina at Chapel Hill, North Carolina

Abstract: Tourette syndrome (TS) is a neurological disorder that causes uncontrolled repetitive motor and vocal tics in children. Examining the neural basis of TS churned out different research studies that advanced our understanding of the brain pathways involved in its development. Particularly, growing evidence points to abnormalities within the fronto-striato-thalamic pathways. In this study, we combined Tract-Based Spatial Statistics (TBSS) and Atlas-based regions of interest (ROI) analysis approach, to investigate the microstructural diffusion changes in both deep and superficial white matter (SWM) in TS children. We then characterized the altered microstructure of white matter in 27 TS children in comparison with 27 age- and gender-matched healthy controls. We found that fractional anisotropy (FA) decreases and radial diffusivity (RD) increases in deep white matter (DWM) tracts in cortico-striato-thalamo-cortical (CSTC) circuit as well as SWM. Furthermore, we found that lower FA values and higher RD values in white matter regions are correlated with more severe tics, but not tics duration. Besides, we also found both axial diffusivity and mean diffusivity increase using Atlas-based ROI analysis. Our work may suggest that microstructural diffusion changes in white matter is not only restricted to the gray matter of CSTC circuit but also affects SWM within the primary motor and somatosensory cortex, commissural and association fibers. *Hum Brain Mapp 37:1903–1919, 2016.*

Contract grant sponsor: National Natural Science Foundation of China; Contract grant numbers: 61271151, 91520202, 31271161; Contract grant sponsor: Youth Innovation Promotion Association CAS and Beijing Municipal Administration of Hospitals Incubating Program; Contract grant number: PX2016035

*Correspondence to: Huiguang He, State Key Laboratory of Management and Control for Complex Systems, Institute of Automation, Chinese Academy of Sciences, Beijing 100190, China. E-mail: huiguang.he@ia.ac.cn and Yun Peng, Department of Radiology, Beijing Children's Hospital, Capital Medical University. No.56 Nanlishi Road, West District, Beijing 100045, China. E-mail: ppengyun@yahoo.com
The first two authors contributed equally to this work.

Received for publication 6 May 2015; Revised 14 January 2016; Accepted 8 February 2016.
DOI: 10.1002/hbm.23146
Published online 1 March 2016 in Wiley Online Library (wileyonlinelibrary.com).

Key words: Tourette syndrome; tract-based spatial statistics; atlas-based ROI analysis; large deformation diffeomorphic metric mapping; superficial white matter

INTRODUCTION

Tourette syndrome (TS) is a developmental neuropsychiatric disorder and is characterized by multiple motor and vocal tics. In general, TS manifests in childhood with a male to female ratio of 5:1. Onset of TS occurs usually with simple motor tics at around 5 years while onset of vocal tics occurs around 8–15 years. Tic severity peaks in early to mid-adolescence and comparatively less in adulthood [Perera and Abayanayaka, 2012]. TS is frequently concomitant with obsessive-compulsive disorder (OCD), attention-deficit–hyperactivity disorder (ADHD) and other social and behavioral disturbances [Stokes et al., 1991].

To date, the neural basis of TS remains largely unknown. However, increasing evidence from experimental, electrophysiological and imaging studies points to abnormalities within the fronto-striato-thalamic pathways [Ganos et al., 2013; Gerard and Peterson, 2003; Makki et al., 2008; McNaught and Mink, 2011; Singer and Minzer, 2003]. Specifically, a dysfunction of the cortico–striato–thalamo–cortical (CSTC) circuit in TS patients has been supported by converging data from neuro-pathological, electrophysiological as well as structural and functional neuroimaging studies [Ackermans et al., 2008; Albin and Mink, 2006; Bronfeld and Bar-Gad, 2013; Harris and Singer, 2006; Mink, 2006]. Furthermore, numerous past studies on this pathophysiology focused on studying gray and white matter regions. For instance, thinning of cortical motor areas as well as reduced caudate nucleus volumes have been reported and interpreted as reflections of altered cortico-subcortical circuits involved in tic generation [Hyde et al., 1995; Peterson et al., 2003]. Moreover, cortical thinning correlating with tic severity was found in the cingulate area as well as supplementary motor, premotor, somatosensory and dorsal lateral prefrontal cortex [Draganski et al., 2010; Muller-Vahl et al., 2009; Peterson et al., 2001; Sowell et al., 2008; Worbe et al., 2012].

Diffusion Tensor Imaging (DTI) is becoming widely used for its high sensitivity in non-invasively detecting microstructural alterations and reconstructing white matter tracts via estimating main fiber orientation [Basser et al., 1996; Basser and Pierpaoli, 1994; Huppi and Dubois, 2006]. Several informative measures can be derived from DTI scans, including fractional anisotropy (FA), mean diffusivity (MD), axial diffusivity (AD) and radial diffusivity (RD). For instance, FA is a sensitive measure of WM microstructural changes, but it is not a specific marker for a certain pathophysiologic mechanisms [Basser, 1995; Basser and Jones, 2002]. MD is sensitive to the microstructural architecture of cellular membranes. Increases in the average spacing between membrane layers increases MD values. RD is modulated by myelin in white matter as suggested in animal research [Song et al., 2005; Tyszka et al., 2006]. AD might be more suited to examine axonal degeneration [Song et al., 2003] and decreases in AD were correlated with increased axonal damage [Budde et al., 2009].

Despite its various promising potentials, using DTI-based analysis methods to calculate local changes across different groups may not be accurate and efficient such as using voxel-based analysis which is highly sensitive to registration errors and suffers from poor statistical power due to high noise levels [Faria et al., 2010]. An alternative approach called Tract-Based Spatial Statistics [Smith et al., 2009] nicely reduces the effects of local misregistrations by skeletonizing the WM and condensing the nearby WM information into a skeleton that approximates WM tract centers. TBSS has been widely adopted using the original implementation provided in the FMRIB Software Library (FSL) [Jenkinson et al., 2012]. Another approach, atlas-based regions of interest (ROI) analysis is also widely used in DTI analyses. It overcomes the shortcomings of voxel-based analysis by grouping the anatomically related voxels within the same anatomical unit, thus systematically lead to higher statistical power. The atlas-based method is also better than manually defining the ROIs,

Abbreviations

AD	Axial diffusivity
ADHD	Attention-deficit–hyperactivity disorder
AIR	Automated Image Registration
ATR	Anterior thalamic radiations
CG	Cingulum bundles
CSTC	Cortico-striato-thalamo-cortical
DTI	Diffusion Tensor Imaging
DWM	Deep white matter
FA	Fractional anisotropy
FOV	Field of view
FSL	FMRIB Software Library
FX	fornices
GM	Gray matter
LDDMM	Large deformation diffeomorphic metric mapping
MD	Mean diffusivity
OCD	Obsessive-compulsive disorder
RD	Radial diffusivity
ROI	Regions of interest
SWM	Superficial white matter
TBSS	Tract-Based Spatial Statistics
TE	Echo time
TFCE	Threshold-free cluster enhancement
TR	Repetition time
TS	Tourette syndrome;
WM	White matter
YGTSS	Yale Global Tic Severity Scale

TABLE I. Demographic variables and clinical characteristics of patients

							Motor tics		Vocal tics	
ID	Sex	Age(y)	YGTSS	Duration(years)	ADHD	OCD	Simple	Complex	Simple	Complex
1	F	11	52	4	No	No	+	+	+	-
2	M	14	65	1.5	Yes	No	+	+	+	+
3	M	6	23	0.25	Yes	No	+	+	-	-
4	M	10	80	2	Yes	No	+	+	+	-
5	M	7	50	0.67	No	No	+	+	-	-
6	M	11	30	2	Yes	No	+	+	-	-
7	M	11	25	1	No	No	+	+	-	-
8	F	5	52	0.25	Yes	No	+	+	+	-
9	M	11	30	1.2	No	No	+	+	-	-
10	M	9	62	2.5	No	No	+	+	+	-
11	F	9	36	5.5	No	No	+	+	-	-
12	F	8	10	0.63	No	No	+	+	-	-
13	M	3	38	0.17	No	No	+	+	+	-
14	M	4	58	1	No	No	+	+	+	-
15	F	8	42	3	No	No	+	+	+	-
16	M	10	30	3	No	No	+	+	+	-
17	M	6	52	0.17	No	No	+	+	+	-
18	M	12	51	2	No	No	+	+	+	-
19	M	11	24	1	No	No	+	+	-	-
20	M	9	55	1.75	No	No	+	+	+	-
21	F	13	76	1.5	No	No	+	+	+	-
22	M	4	35	0.42	Yes	No	+	+	-	-
23	M	9	35	1	No	No	+	+	+	-
24	M	7	59	2.3	No	No	+	+	+	-
25	M	6	42	2.5	Yes	No	+	+	+	-
26	F	4	66	0.25	No	No	+	+	+	-
27	M	16	79	3.5	No	No	+	+	+	-

Abbreviations: + = present, − = absent; YGTSS = Yale Global Tic Severity Scale; M = male; F = female.

which is known to have reproducibility issues and not suitable for the whole-brain analyses since it is time-consuming to define a large number of 3D ROIs. Indeed, previous DTI studies on WM-related diseases used the atlas-based ROI analysis to compare findings from various conditions using statistics calculated from data taken from several individual regions [Faria et al., 2010; Kasahara et al., 2012; Oishi et al., 2009]. In our study, we attempted to overcome the limitations of single analytical approaches by using these two different DTI processing techniques. Thus, studying the brain as a skeleton as well as a partition of anatomical regions will give us a more complete view of its alterations in TS patients.

Studies based on white matter atlases suggest that applying similar techniques (i.e. atlas-based analysis methods) may help us better evaluate microscopic changes in early TS children. Notably, DTI-based studies for examining white matter (WM) components of cortical projections [Cheng et al., 2014] and altered connectivity patterns in TS patients are still scarce. Recently, [Worbe et al., 2015] used a probabilistic tractography algorithm to quantify structural and connectivity changes in CSTC as well as WM microstructure using DTI, where they proved that cortical regions had abnormal structural connectivity with the striatum and the thalamus in TS patients. Despite its elegance, this method was limited to examining only CSTC circuit and its connection to 68 cortical regions. In this study, we use both TBSS and atlas-based method to quantify both superficial and deep white matter (DWM) microstructural changes in 176 ROIs. We also determine whether these changes are related to clinical measures such as YGTSS (Yale Global Tic Severity Scale) and duration of the disease. We hypothesize that WM changes (lower FA, AD and higher RD, MD) would include the SWM of frontal cortices striatum, thalamus and the DWM tracts in CSTC circuit [i.e., cingulum bundles (CG), fornices (FXs) and anterior thalamic radiations (ATR)] in TS children. We also investigate the commissural and association fibres and sensory-motor pathways morphometric changes and their association with tic severity and duration [Liu et al., 2013].

MATERIAL AND METHODS

Subjects

33 TS patients were recruited from outpatient clinics in Beijing Children's Hospital from July 2012 to August 2013.

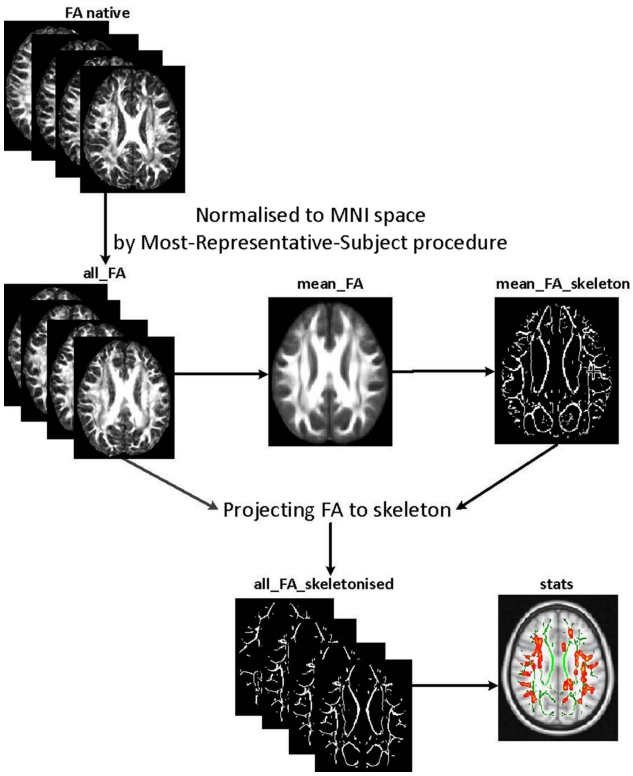

Figure 1.
Flow-chart of the Most-Representative-Subject TBSS (RS-TBSS) procedure. [Color figure can be viewed in the online issue, which is available at wileyonlinelibrary.com.]

All the patients met DSM-IV-TR (Diagnostic and Statistical Manual of Mental Disorders, 4th Edition, text revision) criteria for TS. We also included 48 healthy controls in our study. We used a clinical interview and the Children's Yale-Brown Obsessive Compulsive Scale (CY-BOCS) [Scahill et al., 1997] to diagnose OCD and used the German short version of Wender Utah rating scale (WURS-k, translated to Chinese) [Retz-Junginger et al., 2003] to diagnose ADHD. Patients fulfilling OCD criteria or other co-morbidities were excluded from the study. Only 27 TS patients (age: 9.00 ± 3.374 years, range: 3–16 years; 7 female) and 27 age and gender-matched control subjects (age: 10.74 ± 3.323 years; range: 6–17 years; 11 female) were included in this paper. There is no medical treatment for all patients. Tic severity for all patients was rated using the Yale Global Tic Severity Scale (YGTSS) [Leckman et al., 1989] and ranged from 10 to 79 ([mean ± SD]: 46.50 ± 18.037). The duration of TS ranged from 3 month to 5 years ([mean ± SD]: 1.81 ± 1.423 years). For those who had course less than 1 year, TS diagnosis was made by follow-up call. After the study was approved by Beijing Children's Hospital review board, written informed consent was obtained from all the parents/guardians according to the Declaration of Helsinki. Details of the patients are shown in Table I.

Data Acquisition

Magnetic resonance imaging was acquired using a 3.0T MR scanner (Gyroscan Interna Nova, Philips, Netherland). Head positioning was standardized using canthomeatal landmarks. The head was stabilized with foam pads to minimize head movements. Patients were instructed to suppress tics and minimize head movements during scanning as much as possible. Children with mild symptoms of tics can control their tics, therefore minimizing the risk to get motion artifacts. For children with serious tic symptoms, we perform scanning after they sleep. In the scanning process, the physician observes the patient via the monitor to ensure that the patient remains still. Axial three-dimensional DTI was acquired from all the subjects. DTI was performed using the following protocol: spin-echo diffusion-weighted echo-planar imaging sequence, 2mm slice thickness, no inter-slice gap, repetition time = 4,300 ms, echo time = 95ms, field of view (FOV) = 255×255mm, reconstructed image matrix = 336×336. Diffusion MRI images were obtained from 30 non-collinear directions with a b value of 1,000 s/mm^2. 3D T1-weighted imaging were performed with axial three-dimensional-Fast Field Echo (3D FFE) sequence with the following parameters: repetition time (TR) = 25ms, echo time (TE) = 4.6ms, flip angle = 30°, reconstructed image matrix = 256×256, FOV = 200×200mm, slice thickness = 1mm.

Data Preprocessing

Following image acquisition, we used the FMRIB's Diffusion Toolbox (FDT2.0) within FSL v4.1 (http://www.fmrib.ox.ac.uk/fsl) for diffusion tensor image processing. For each participant, 30 DTI volumes with 1,000 s/mm^2 b-value were first affinely registered to the b0 volume for correction of eddy current distortion and simple head motion. Non-brain voxels were removed using FSL Brain Extraction Tool (BET). We thresholded the FA map at 0.25 to generate a binary brain mask for each subject. We then used the eddy-corrected 4D data and corresponding brain mask to fit the diffusion tensor model at each voxel by using the FDT. Eigenvalues of diffusion tensor matrix (λ_1, λ_2, λ_3) were obtained and maps of axial diffusivity ($AD = \lambda_1$), mean diffusivity ($MD = (\lambda_1+\lambda_2+\lambda_3)/3$), and FA were generated. RD (perpendicular eigenvalue, $\lambda_{23} = (\lambda_2+\lambda_3)/2$) was calculated by averaging λ_2 and λ_3 maps.

Quantification of Microstructural Changes with TBSS

The Most-Representative-Subject TBSS (RS-TBSS) procedure [Shiva et al., 2012] was then applied to the data (Flow-chart is shown in Fig. 1), which is recommended if the subjects are all young children. FA images from each participant were then co-registered to one another using both linear (FLIRT) and nonlinear registration (FNIRT)

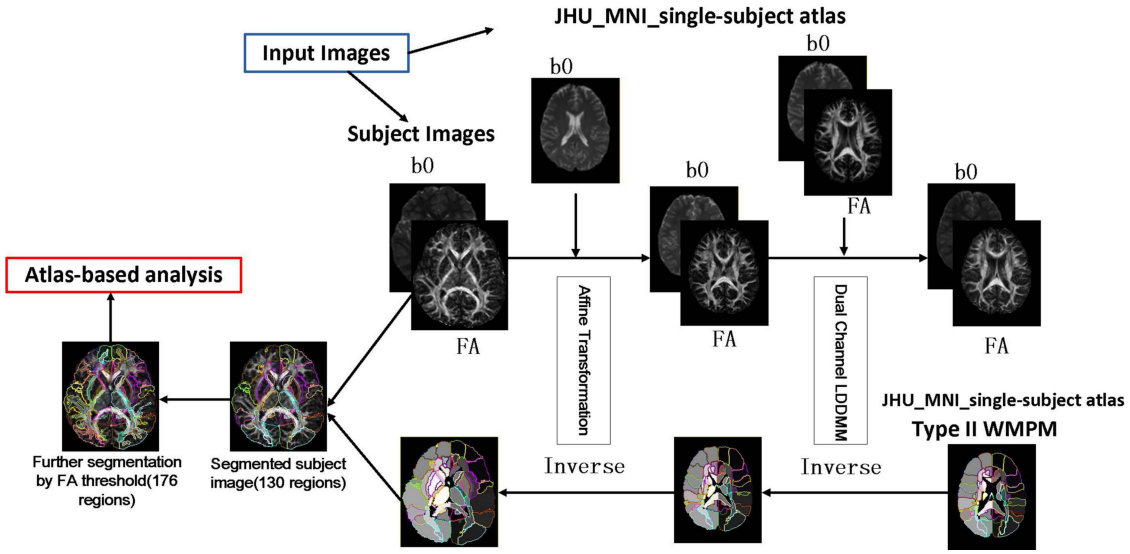

Figure 2.

Schematic diagram of dual-contrast LDDMM Atlas-based analysis pipeline. FA and b0 maps of each participant were first transformed linearly and then non-linearly to "JHU_MNI_single-subject" atlas. Next, the inverse transformation was applied to the pre-segmented WM atlas, thus enabling automated segmentation of the original images into 130 subregions. The cortex and the associated SWM were further divided using a threshold (FA > 0.25) for each subject, resulting in a total of 176 subregions. [Color figure can be viewed in the online issue, which is available at wileyonlinelibrary.com.]

provided by FSL. Next, we select the subject that has the minimum mean deformation for non-linearly aligning it to all subjects as the "most representative" one, and use it as the target image. This target image is then affine-registered to MNI152 standard space where each image is transformed into $1 \times 1 \times 1$ mm by combining the nonlinear transform to the target FA image with the affine transform from that target to MNI152 space. We used the adult atlas (FMRIB58_FA) for the purpose of normalizing all data to a common stereotactic space (MNI152 space). Burgund et al. examined the spatial error that occurred when the brains of children and adults were warped to an adult template using affine registration. They found that there were small errors of registration between children and adults [Burgund et al., 2002]. The resulting standard-space FA images of each participant were averaged to create a mean FA image, which was then fed into an FA skeletonization program to create a skeleton image of WM tracts. A threshold of 0.2 was selected to define the border distinguishing white from gray matter (GM). Then, for each participant, we projected the local maximal FA value [Bach et al., 2014; de Groot et al., 2013] along the perpendicular direction of the WM tract to the mean FA skeleton to carry out the voxel wise statistics across subjects. The same projection method was applied to MD, AD, and RD images. For voxel-wise group comparisons between patients and normal control on the skeleton image, we used FSL's *randomise* tool. Essentially, *randomise* uses a permutation-based statistical inference [Nichols and Holmes, 2002]. Random Monte Carlo simulated samples of 10,000 permutations were used as null distribution. P-values < 0.05 were identified as significant and corrected for multiple comparisons with threshold-free cluster enhancement (TFCE) [Smith and Nichols, 2006] method to avoid definition of an initial cluster-forming threshold or carrying out a large amount of data smoothing. The *ICBM-DTI-81 white-matter labels* atlas, *JHU White-Matter Tractography* atlas and *Talairach Daemon Labels* atlas provided by FSL were used to identify the abnormal white matter tracts using TBSS. Similarly, we also analyze MD, RD and AD TBSS results.

Atlas-Based ROI Statistical Analysis Using LDDMM

Brain parcellation into 176 ROIs using LDDMM atlas-based registration framework

In atlas-based ROI analysis, we use the pre-parcellated template brain to transfer template regions labels to a target unparcellated brain. Despite its robustness, this direct approach produces measurements whose performance critically depends on the accuracy of the image registration. In this study, we use a nonlinear warping algorithm based on large deformation diffeomorphic metric mapping (LDDMM) [Miller et al., 1993; Miller et al., 1997] to register DTI images of each participant to common space. LDDMM accurately estimates a large degree of deformation while simultaneously preserving the topology of the object, thus

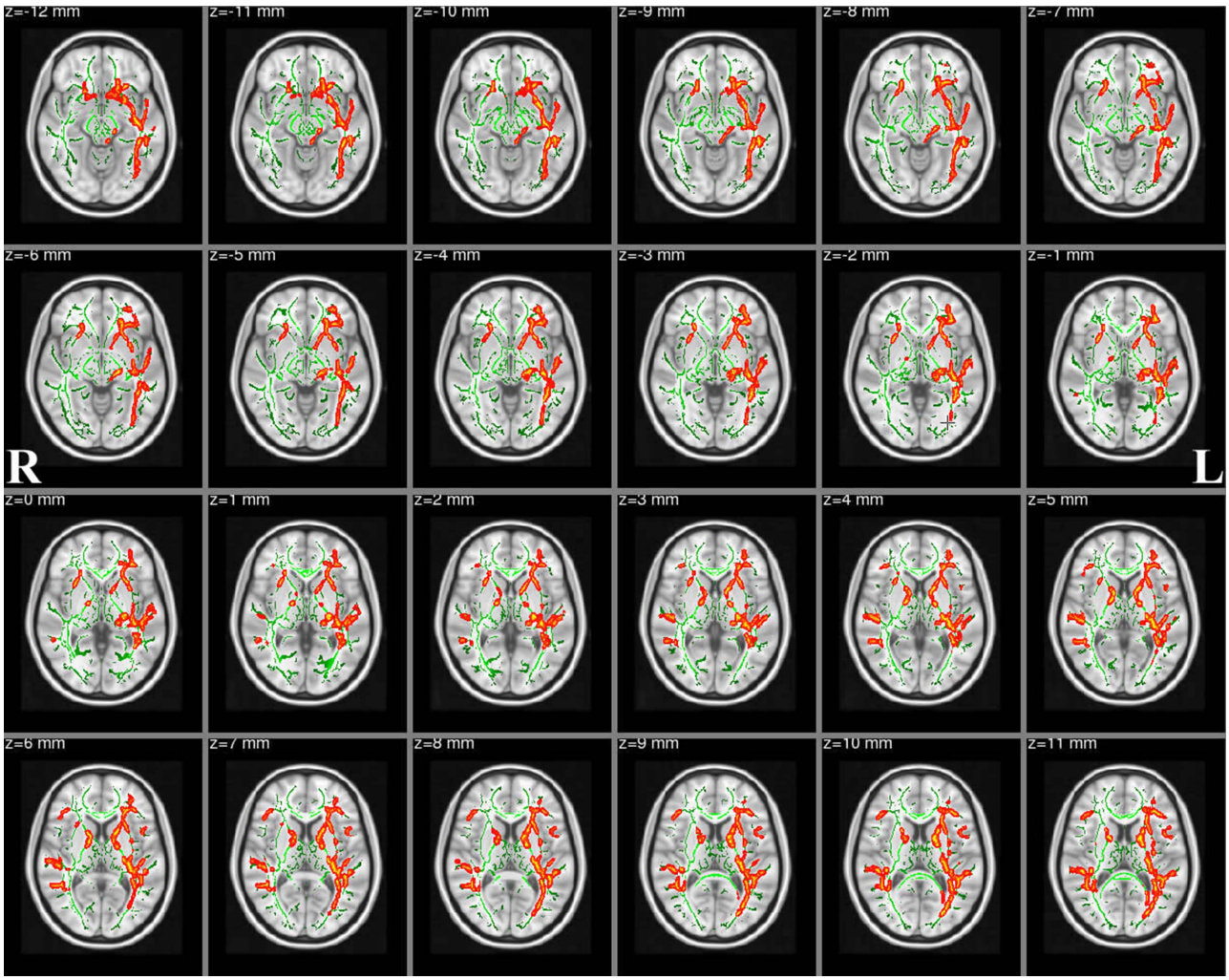

Figure 3.

FA skeleton clusters at $P < 0.05$ (family-wise error corrected for multiple comparisons). We overlay the FA skeleton (green) on axial slices of the standard MNI_T1_1mm template. Red-Yellow voxels represent regions with significantly decreased FA values in Tourette syndrome patients relative to healthy controls. The white-matter microstructure is altered in the body of corpus callosum, forceps major, left superior longitudinal fasciculus, ATR/superior cerebellar peduncle, right superior longitudinal fasciculus (temporal part), inferior longitudinal fasciculus, inferior fronto-occipital fasciculus and corticospinal tract. [Color figure can be viewed in the online issue, which is available at wileyonlinelibrary.com.]

constraining transformations such that connected tissues remain connected and distinct (different) tissues are not joined. In this study, we used multi-contrast LDDMM algorithm was implemented, in which both scalar-valued diffusion weighted images and anisotropy images obtained from DTI data to drive the registration with their different contrast information [Ceritoglu et al., 2009].

A two-step image transformation was used to warp an atlas to individual native space. We used the adult skull-stripped "JHU_MNI_single-subject" atlas [Oishi et al., 2009] for linear and nonlinear normalization of subject images and we generated ROIs for each participant as follows (Flow-chart is shown in Fig. 2). Basically, the images for each participant were first normalized to the MNI-space using a 12-parameter affine transformation (affine Automated Image Registration (AIR) transformation, with trilinear interpolation) based on b0 images for both the subject data and the template. We then used both b_0 and FA images for dual-contrast LDDMM (with cascading alpha of 0.01, 0.005, and 0.002) warping the subject data into the b0 and FA template. The inverse transformation matrices (inverse LDDMM and then inverse AIR, all with nearest neighbor interpolation) were then used to transfer back the pre-segmented WM atlas "Type II WM

TABLE II. Skeleton clusters showing significantly decreased FA at $P < 0.05$ (corrected for multiple comparisons with TFCE)

Tract	Cluster size	*P*-value	MNI Coordinates(mm)		
			x	y	z
Body of corpus callosum	1,670	0.037	0	−22	24
Forceps major	230	0.047	26	−68	30
	22	0.049	−10	−94	7
	14	0.05	23	−78	20
Right superior longitudinal fasciculus (temporal part)	13,460	0.023	40	−48	17
Right inferior longitudinal fasciculus	430	0.049	33	−77	0
	14	0.05	46	−6	−15
Right inferior fronto-occipital fasciculus	154	0.046	40	−12	−14
Right corticospinal tract	8	0.049	0	−42	−46
Left superior longitudinal fasciculus	18,617	0.014	−34	−9	39
Left frontal lobe sub-gyral	164	0.046	−30	21	35
Left ATR	86	0.049	−6	−46	−27

MNI: Montreal Neurological Institute.

Parcellation Map (WMPM)"[Oishi et al., 2009] to each subject native space, thus enabling the automated segmentation of the data into 130 brain regions. The cortex and the white matter were further divided using an FA threshold set to 0.25, which eventually resulted in a total of 176 subregions. We also calculated the regional diffusion metrics (FA, MD, AD, and RD) by averaging the values within each region using ROIEditor.

Statistical analysis of DTI-derived regions of interest

The Shapiro–Wilk Test of Normality was used to investigate the data distribution. The majority of WM measures had normal distributions in both TS and control groups. Using the two-sample *t-test*, the mean regional AD, RD, MD and FA values in the patient group were compared with those in the control group using SPSS19.0. For non-normally distributed variable, we conducted non-parametric analysis (Mann–Whitney U tests). The *P*-values <0.05 were regarded as significant in our analysis.

Linking Changes to Clinical Measures

We calculated partial correlation using SPSS to relate corresponding values of abnormal WM ROIs to tic severity score (YGTSS) and tics duration, controlling for age and gender. The region with abnormal values as identified by TBSS or atlas-based analysis were selected as ROIs.

RESULTS

TBSS Analysis

TBSS analyses revealed significantly reduced FA in multiple WM skeleton clusters of patients, including the body of the corpus callosum, the forceps major, the left superior longitudinal fasciculus, the ATR, the right superior longitudinal fasciculus (temporal part), the inferior longitudinal fasciculus, the inferior fronto-occipital fasciculus, the orticospinal tract and the frontal lobe sub-gyral (Fig. 3). The coordinates of the cluster local maxima and the cluster size are listed in Table II. We did not find any significant FA increases compared with the healthy control subjects. Nonetheless, we found significantly increased RD in the left inferior fronto-occipital fasciculus, the right putamen and the contralateral superior longitudinal fasciculus (Fig. 4). The coordinates of the local maxima and cluster size are listed in Table III. We did not find any significant RD decreases compared with the healthy control subjects. Furthermore, skeleton clusters showed no significantly different MD/AD at $P < 0.05$.

Atlas-Based ROI Analysis

Compared to healthy controls, TS patients showed significant differences in multiple WM regions that extend CSTC circuit (see Tables IV and V). Furthermore, FA, AD were reduced and RD, MD were increased in these white matter regions (only except for left posterior corona radiata and middle occipital WM, with increased AD) in TS patients than in control group (see Fig. 5).

Structural Changes in Relation to Clinical Measures

To examine the functional relevance of the identified structural changes, we correlated microstructural measures with two clinical parameters: tic severity score (YGTSS) and tic duration.

In TBSS analysis, FA values in the forceps major ($r = -0.479$, $P = 0.015$), right inferior longitudinal fasciculus ($r = -0.577$, $P = 0.003$), right inferior fronto-occipital

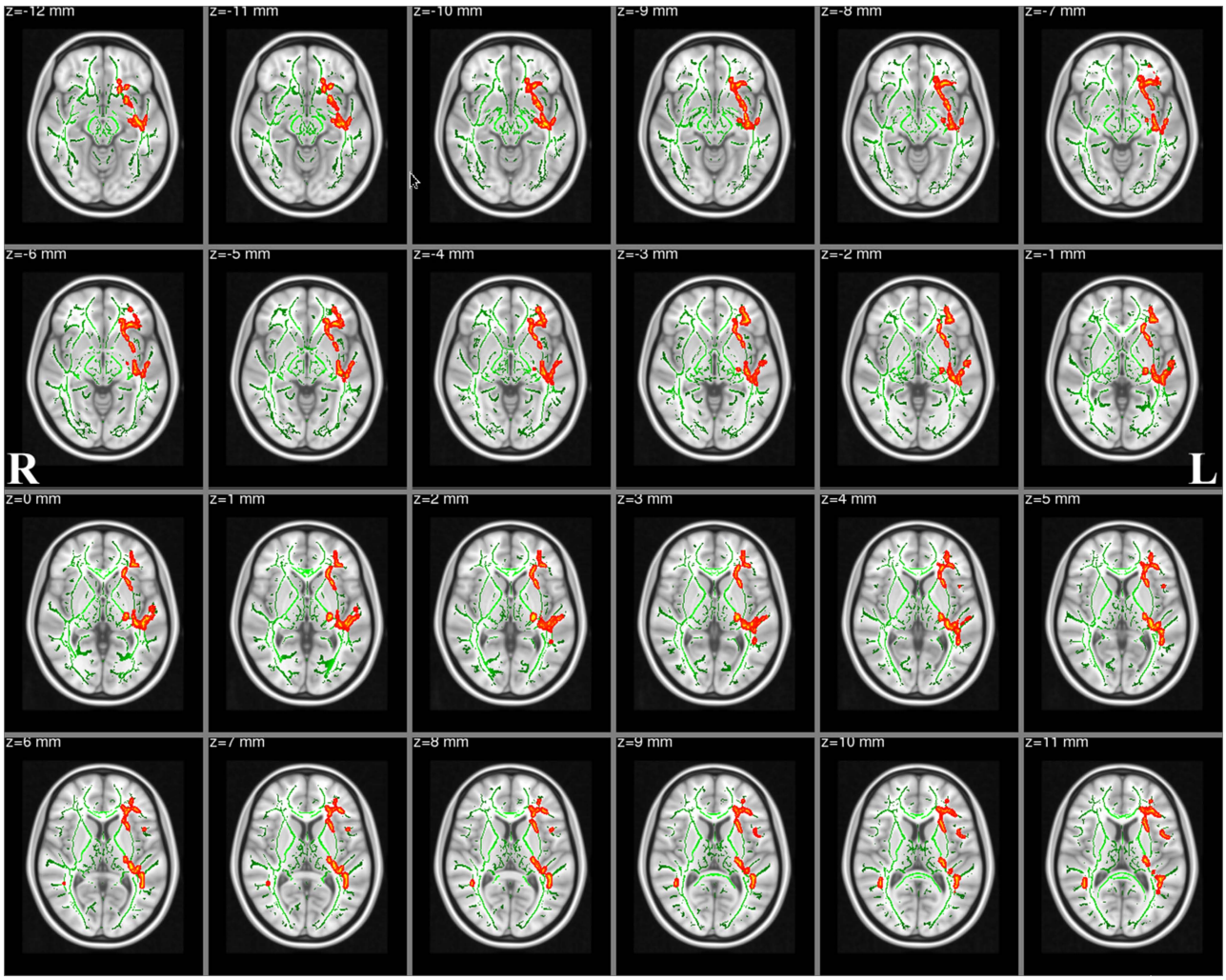

Figure 4.

White matter structures showing significantly increased RD in Tourette syndrome patients (corrected for multiple comparisons, $P < 0.05$). We overlay the RD skeleton (green) on the standard MNI_T1_1mm template. Red-Yellow voxels represent regions in which RD significantly increased in Tourette syndrome patients relative to healthy controls. [Color figure can be viewed in the online issue, which is available at wileyonlinelibrary.com.]

TABLE III. Skeleton clusters showing the significantly increased RD at $P < 0.05$ (corrected for multiple comparisons with TFCE)

Tract	Cluster size	*P*-value	MNI Coordinates(mm)		
			x	y	z
Right inferior fronto-occipital fasciculus	2,011	0.044	28	22	21
Right superior longitudinal fasciculus	338	0.048	37	−1	37
	21	0.05	51	−3	17
	16	0.05	58	−5	14
Right Putamen	25	0.05	16	13	−13
Left superior longitudinal fasciculus	25,759	0.024	−40	−47	15

MNI: Montreal Neurological Institute.

TABLE IV. List of group statistics on FA, AD, RD, MD for all abnormal superficially located white matter regions

ROI	*P*-value/variation direction				
	FA	AD	RD	MD	
Superior frontal WM left	0.009↓	N.S.	N.S.	N.S.	SFWM_L
Inferior frontal WM left	0.003↓	N.S.	0.023↑	N.S.	IFWM_L
Precentral WM left	0.001↓	N.S.	0.015↑	N.S.	PrCWM_L
Postcentral WM left	0.004↓	N.S.	0.034↑	N.S.	PoCWM_L
Angular WM left	0.008↓	N.S.	0.038↑	N.S.	AWM_L
Pre-cuneus WM left	N.S.	N.S.	0.027↑	N.S.	PreCuWM_L
Fusiform WM left	N.S.	N.S.	0.035↑	N.S.	FuWM_L
Middle occipital WM left	N.S.	0.014↑	N.S.	0.029↑	MOWM_L
Superior temporal WM left	0.023↓	N.S.	0.028↑	0.041↑	STWM_L
Inferior temporal WM left	0.033↓	N.S.	N.S.	N.S.	ITWM_L
Middle temporal WM left	N.S.	N.S.	0.029↑	0.017↑	MTWM_L
Lateral fronto-orbital WM left	<0.001↓	0.033↓	0.004↑	N.S.	LFOWM_L
Supramarginal WM left	0.029↓	N.S.	0.031↑	0.043↑	SMWM_L
Superior parietal WM right	N.S.	N.S.	N.S.	0.028↑	SPWM_R
Superior frontal WM right	0.011↓	N.S.	N.S.	N.S.	SFWM_R
Middle frontal WM right	0.015↓	N.S.	N.S.	N.S.	MFWM_R
Inferior frontal WM right	0.026↓	N.S.	N.S.	N.S.	IFWM_R
Precentral WM right	0.012↓	N.S.	0.033↑	N.S.	PrCWM_R
Postcentral WM right	0.015↓	N.S.	0.034↑	N.S.	PoCWM_R
Pre-cuneus WM right	0.03↓	N.S.	N.S.	N.S.	PreCuWM_R
Middle occipital WM right	0.008↓	N.S.	0.016↑	0.035↑	MOWM_R
Superior temporal WM right	0.031↓	N.S.	N.S.	N.S.	STWM_R
Middle temporal WM right	0.023↓	N.S.	N.S.	N.S.	MTWM_R
Supramarginal WM right	0.024↓	N.S.	N.S.	N.S.	SMWM_R
Rectus WM right	0.008↓	N.S.	N.S.	N.S.	RWM_R

FA, AD were reduced and RD, MD were increased in TS group in all regions, except in the middle occipital WM where AD increased. WM: white matter, N.S.: not significant, ↑/↓: parameter is significantly increased/decreased in TS group compared to control group.

fasciculus ($r = -0.441$, $P = 0.027$), left ATR ($r = -0.552$, $P = 0.004$) and left superior longitudinal fasciculus ($r = -0.442$, $P = 0.027$) were significantly negatively correlated with YGTSS scores of the patient group (Fig. 6A). RD values in the right inferior fronto-occipital fasciculus ($r = 0.405$, $P = 0.044$), left superior longitudinal fasciculus ($r = 0.535$, $P = 0.006$) and left superior longitudinal fasciculus($r = 0.512$, $P = 0.009$) were significantly positively correlated with YGTSS scores of the patient group (Fig. 6B). No correlation between FA, RD changes and tic duration was found.

In the atlas-based ROI analysis for deep WM tracts, FA values in the left cingulum bundle projecting to the cingulate gyrus ($r = -0.414$, $P = 0.039$), left sagittal stratum ($r = -0.603$, $P = 0.001$), left external capsule ($r = -0.422$, $P = 0.036$), left splenium of corpus callosum ($r = -0.405$, $P = 0.045$), right superior cerebellar peduncle ($r = -0.413$, $P = 0.040$), right genu of corpus callosum ($r = -0.450$, $P = 0.024$) were significantly negatively correlated with YGTSS scores of the patient group (Fig. 7A); whereas, RD and MD values in the left superior longitudinal fasciculus ($r = 0.426$, $P = 0.034$ and $r = 0.460$, $P = 0.021$) were significantly positively correlated with YGTSS scores of the patient group (Fig. 7B). We did not find any significant correlation between AD values and YGTSS scores. Meanwhile all DT metrics had no significant correlation with tic duration.

For superficial WM, after controlling for age and gender, FA values in the right pre-cuneus WM ($r = -0.558$, $P = 0.004$) and the right superior temporal WM ($r = -0.448$, $P = 0.025$) were significantly negatively correlated with YGTSS scores of the patient group (Fig. 7C). For the basal ganglia and the thalamus, after controlling for age and gender, FA values in the left thalamus ($r = -0.413$, $P = 0.040$) and the left caudate nucleus ($r = -0.531$, $P = 0.006$) were significantly negatively correlated with YGTSS scores of the patient group (Fig. 7D).

DISCUSSION

In this study, we combined TBSS and atlas-based ROI analysis to examine both superficial and DWM structural and microstructural changes in TS patients with short disease duration without OCD. We found widespread structural alterations in TS children brain using both methods while a previous study [Jeppesen et al., 2014] selected seven ROIs on the WM skeleton and found no difference between controls and TS patients in these regions

TABLE V. List of group statistics on FA, AD, RD, MD for all abnormal deep white matter, thalamus and basal ganglia

	P-value/variation direction				
	FA	AD	RD	MD	
Caudate nucleus left	0.018↓	N.S.	N.S.	N.S.	Caudate_L
Putamen left	0.028↓	N.S.	N.S.	N.S.	Putamen_L
Superior cerebellar peduncle left	0.023↓	N.S.	0.004↑	0.007↑	SCP_L
Cerebral peduncle left	0.035↓	N.S.	N.S.	N.S.	CP_L
Anterior limb of internal capsule left	0.004↓	0.003↓	N.S.	N.S.	ALIC_L
Posterior limb of internal capsule left	0.034↓	N.S.	N.S.	N.S.	PLIC_L
Anterior corona radiata left	0.025↓	N.S.	N.S.	N.S.	ACR_L
Posterior corona radiata left	N.S.	0.045↑	N.S.	N.S.	PCR_L
Cingulum cingulate gyrus left	0.006↓	N.S.	0.018↑	N.S.	CGC_L
Superior longitudinal fasciculus left	N.S.	N.S.	0.035↑	0.036↑	SLF_L
Superior fronto-occipital fasciculus left	0.01↓	N.S.	N.S.	N.S.	SFO_L
Inferior fronto-occipital fasciculus left	0.005↓	N.S.	0.045↑	N.S.	IFO_L
Sagittal stratum left	0.049↓	N.S.	0.037↑	0.042↑	SS_L
External capsule left	0.007↓	N.S.	N.S.	N.S.	EC_L
Uncinate fasciculus left	0.031↓	N.S.	0.048↑	N.S.	UNC_L
Body of corpus callosum left	0.047↓	N.S.	N.S.	N.S.	BCC_L
Splenium of corpus callosum left	0.041↓	N.S.	N.S.	N.S.	SCC_L
Retrolenticular part of internal capsule left	0.015↓	N.S.	N.S.	N.S.	RLIC_L
Globus pallidus left	0.016↓	N.S.	N.S.	N.S.	*GP_L
Thalamus left	0.02↓	N.S.	N.S.	N.S.	Thalamus_L
Medulla left	N.S.	0.037↓	N.S.	N.S.	Medulla_L
Caudate nucleus right	0.017↓	N.S.	N.S.	N.S.	Caudate_R
Superior cerebellar peduncle right	0.006↓	N.S.	0.023↑	N.S.	SCP_R
Anterior limb of internal capsule right	0.003↓	0.002↓	N.S.	N.S.	ALIC_R
Posterior limb of internal capsule right	0.031↓	N.S.	N.S.	N.S.	PLIC_R
Anterior corona radiata right	0.043↓	N.S.	N.S.	N.S.	ACR_R
Superior corona radiata right	0.023↓	N.S.	N.S.	N.S.	SCR_R
Cingulum cingulate gyrus right	0.037↓	N.S.	0.031↑	N.S.	CGC_R
Superior longitudinal fasciculus right	N.S.	N.S.	N.S.	0.041↑	SLF_R
Superior fronto-occipital fasciculusright	0.018↓	N.S.	0.042↑	N.S.	SFO_R
Inferior fronto-occipital fasciculus right	0.002↓	0.004↓	0.05↑	N.S.	IFO_R
Sagittal stratum right	N.S.	N.S.	0.042↑	N.S.	SS_R
External capsule right	0.014↓	N.S.	N.S.	N.S.	EC_R
Middle cerebellar peduncle right	N.S.	N.S.	0.046↑	N.S.	MCP_R
Genu of corpus callosum right	0.026↓	N.S.	N.S.	N.S.	GCC_R
Splenium of corpus callosum right	0.028↓	N.S.	N.S.	N.S.	SCC_R
tapatum right	0.028↓	N.S.	N.S.	N.S.	TAP_R
pons right	0.049↓	N.S.	0.019↑	N.S.	Pons_R

FA, AD were reduced and RD, MD were increased in TS group in all regions, except in the left posterior corona radiata where AD increased.
WM: white matter, N.S.: not significant, ↑/↓: parameter is significantly increased/decreased in TS group compared to control group, *GP_L: GlobusPalidus_L.

corrected for multiple comparisons with Bonferroni method. The discrepancies of study subjects, analysis method to derive the statistical result and multiple comparisons correction method may play a role in the different findings resulting from both studies. In our result, TS alterations were not only observed within the deep WM tracts but also were present in the CSTC and the SWM beneath the cortex identified by decreasing FA and AD values (observed in both TBSS and atlas-based ROI analysis results) and increasing RD and MD values (noted in only atlas-based ROI analysis results). Our results may suggest a lower axonal density and dysmyelination with potential enlargement of myelin sheets of SWM pathway in patients with TS. Besides increased MD values were observed in TS patients primarily in the temporal WM and association fibers, which could result from a decreased cell density, thereby reflecting a putative pathomechanism of disruption within the temporal WM and association fibers. Increased MD could result in reduced connectivity. No significant change was found in AD

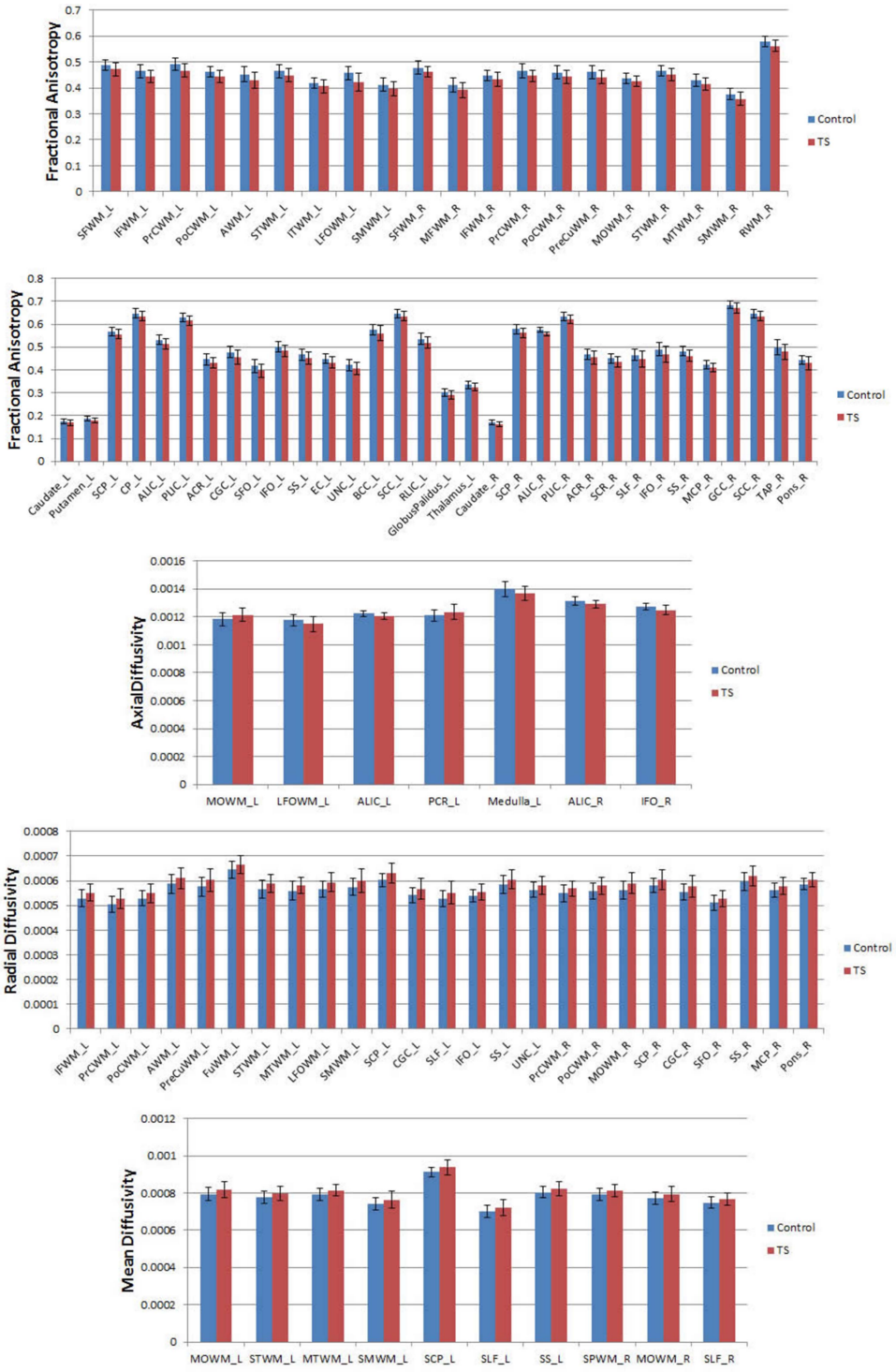

Figure 5.

Significant differences in diffusion measures ($P < 0.05$) using atlas-based analysis of TS and control groups. This figure shows the mean FA, AD, RD and MD from ROI for TS (red) and control (blue) groups. Values represent mean ± standard deviation. Abbreviations of ROIs are in Tables I and II. [Color figure can be viewed in the online issue, which is available at wileyonlinelibrary.com.]

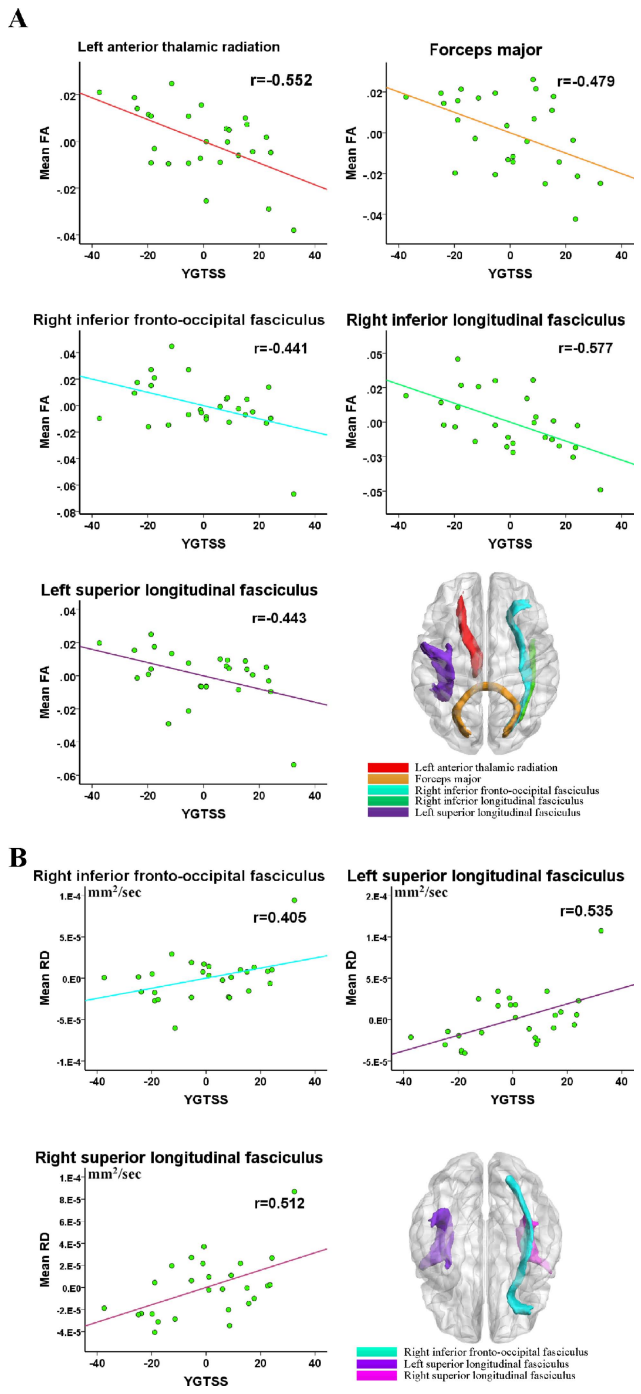

Figure 6.

TBSS correlation analysis results. (A) Significant negative correlation between YGTSS and mean FA values. (B) Significant positive correlation between YGTSS and mean RD values. Of note, the X-axis and Y-axis only reflect the partial correlation of DTI parameter and YGTSS, while considering age and gender as covariables. The coordinate value of both X-axis (YGTSS) and Y-axis (DTI parameter) do not reflect the initial values of these variables. [Color figure can be viewed in the online issue, which is available at wileyonlinelibrary.com.]

values using TBSS, which may show that it not a sensitive DTI parameter in TS children.

Alterations in SWM

Tissue alterations in the SWM are less understood relative to cortical GM and DWM in previous studies of TS. Lying just beneath the cortical ribbon, SWM is composed primarily of U-shaped association fibers, which form the major local white matter connections in the brain arching through the cortical sulci to connect adjacent gyri; also intracortical axons, which extend directly to white matter from the overlying GM. Notably, local white matter connections lie in the SWM [Nazeri et al., 2013] and SWM changes are highly correlated with corresponding changes in the cortex [Nazeri et al., 2013]. To date, much less is known about SWM in vivo in patients in TS children.

In this study, microscopic changes in SWM were evaluated using water diffusion parameters including FA, AD, RD and MD maps. To the best of our knowledge, our study is one of the very few studies to examine the correlation between the SWM alterations and clinical scores as well as duration of tics. In atlas-based analysis, SWM showed primary decreasing FA and increasing RD values underneath bilateral primary somatosensory cortices in TS children, suggesting the structure change of central sensory system after long-term adaptation could tighten controls of tics. Decreasing FA and increasing RD were also found in SWM beneath bilateral precentral, postcentral, fronto-orbital and superior temporal auditory cortices, suggesting decreased axonal coherence. These regions are involved in sensory-motor information processing.

Additionally, FA values in the right precuneus WM and the right superior temporal WM were also significantly negatively correlated with YGTSS scores. It was also noted that the precuneus is involved in self-referential processing, imagery and memory, and its deactivation is associated with an aesthetic-induced loss of consciousness. Converging with previous studies, we found abnormal pathway activity of precuneus and the presence of the abnormal metabolic changes in the region correlated with the severity of a TS patient's symptoms [Alongi et al., 2014; Pourfar et al., 2011]. Furthermore, the superior temporal gyrus regions were significantly correlated with tic occurrence in TS patients [Stern et al., 2000]. Of note, the superior temporal gyrus is an important structure in the pathway consisting of the amygdala and prefrontal cortex, which are all involved in the perception of emotions in facial stimuli [Bigler et al., 2007].

We also found the FA values and RD values changed between groups in the precentral WM and postcentral WM. The precentral WM and postcentral WM, which represent the white matter below the postcentral (BA 3a) and precentral (BA 4p) cortex, were segmented using LDDMM atlas-based method. Very few papers could segment the precentral WM and postcentral WM and study the group

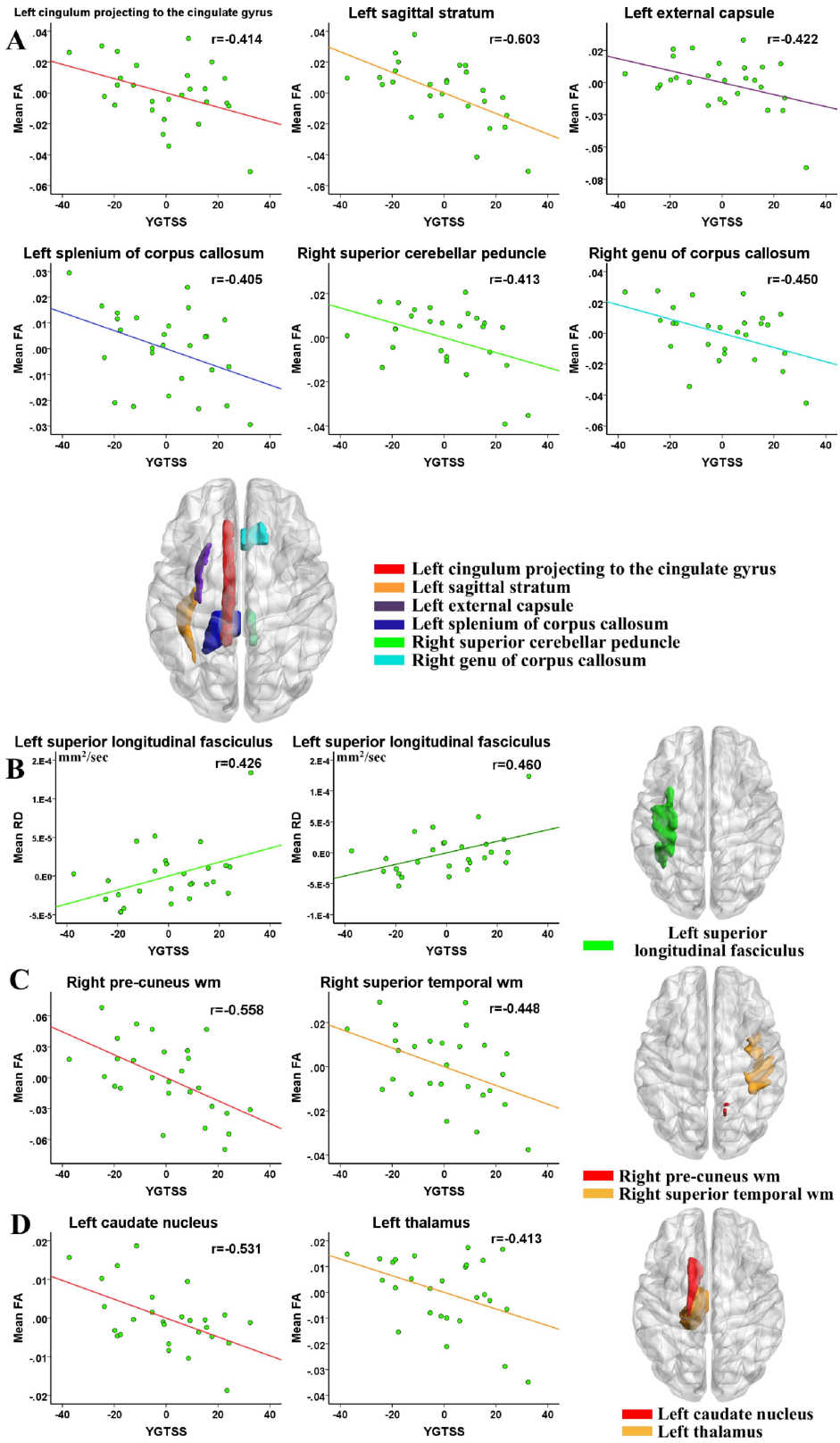

Figure 7.

Atlas-based correlation analysis in deep white matter tracts (DWMT), superficial white matter regions (SWMR) and different nuclei. (A) Significantly negative correlation between YGTSS and mean FA value in DWMT. (B) Significantly positive correlation between YGTSS and mean RD and MD value in DWMT. (C) Significantly negative correlation between YGTSS and mean FA value in SWMR. (D) Significantly negative correlation between YGTSS and mean FA value in left caudate nucleus and thalamus. Of note, the X-axis and Y-axis only reflect the partial correlation of DTI parameter and YGTSS, while considering age and gender as covariables. [Color figure can be viewed in the online issue, which is available at wileyonlinelibrary.com.]

differences in their regional diffusion characteristics. Previous study [Thomalla et al., 2009] found that FA values changed between controls and TS groups in these regions. So far, no post-mortem neuropathology studies of TS were found on precentral WM and postcentral WM.

Alterations in Motor-Sensory Areas, CSTC, Commissural and Association Fibres

Tics are the hallmark of TS; thus, it is intuitive to study the main motor pathway, the corticospinal tract. Decreased FA in the corticospinal tract found by TBSS is in agreement with our hypotheses the corticospinal tract as main motor pathway is affected in TS. FA changes start from the corona radiate (identified using TBSS) and extend to the ATR (identified using atlas-based analysis). In the anterior limb, FA alterations (identified using atlas-based analysis) might affect the frontopontine tract which carries the motor pathways from the frontal lobe to the pons. Furthermore, cortico-striato-thalamo-cortical circuits are believed to be connected directly to the ventral striatum where motivational and incentive behaviors are regulated [Haber and Knutson, 2010]. Our atlas-based analysis showed widespread reduced FA in caudate nucleus, putamen, globus pallidus and thalamus. Striatum in CSTC is the largest component of the basal ganglia which control the velocity and direction of movement and play an important role in the generation of tics [Plessen et al., 2004]. Similar results were found with previous DTI studies [Li et al., 2010; Muller-Vahl et al., 2014]. Abnormal thalamic FA may result in a decreased thalamic output to the frontal cortex and to other components of the CSTC, which could lead to a decreased cortical inhibition leading to an increase in tic frequency. Abnormal FA values in the putamen is suggested as a result of disrupted white matter projections to the globus pallidus. The microstructure change of globus pallidus led to inhibiting the transfer of useful information cannot to the cerebral cortex, causing the tics. For the WM tracts within the CSTC, we found FA reduction in the ATR, which connects the medial thalamic nuclei with the rostral part of the frontal lobe and the cingulate cortex. These altered connections between basal ganglia and the prefrontal, frontal areas is of key importance in the tics' pathophysiologic mechanism in TS [Bohlhalter et al., 2006; Singer, 2005].

In addition, the corpus callosum is the biggest commissural fibers and transfers information between the two hemispheres. The corpus callosum is supposed to play an important role in modulation of tics by mediating the inhibiting influence by prefrontal cortices. The reduced FA values in the corpus callosum in our data could be responsible for a diminished inhibitory influence. Using the atlas-based ROI analysis, we found in all sub-regions of the corpus callosum a reduced FA-value. The differences in FA values were highest in the body portions of the corpus callosum, and lowest in the genu area, confirming the found in previous studies [Cavanna et al., 2010; Plessen et al., 2009], which showed plastic remodeling in the corpus callosum possibly represents an adaptation mechanism in TS.

The modulation of tics by cortical activation depends not only on commissural fibers between interhemispheric but also on long association fiber bundles within one hemisphere [Church et al., 2009] described altered connectivity patterns between the prefrontal, frontal, midcingulate cortex, the precuneus and the inferior parietal gyrus in TS children. Reduced FA and increased RD values were found in superior/inferior longitudinal fasciculus and superior/inferior fronto-occipital fasciculus using both methods. The results were in agreement with our hypotheses that alterations in WM would reach beyond the CSTC as the association fibre bundles are also affected in TS.

Pathological Reasons and Brain Development of TS Children

Our findings associate widespread WM changes with TS children. The alterations are not limited to just one brain area or one system. However, the pathological mechanism of TS children is still unclear hitherto because brain development during childhood is a complex and dynamic process. It is generally believed that abnormalities in genes are responsible for most TS occurrences [Comings et al., 1984; Petek et al., 2001]. A child is more likely to develop Tourette's syndrome if their parent was TS-diagnosed. Studies also suggest that there may be a problem with one of the brain's chemicals called dopamine. Children with neurological defects in the structure and working of the brain thus do not produce enough myelin, or they have metabolic problems that may cause white matter degeneration which were manifested primarily by reduced FA and increased RD values in both methods. Another theories involve in environmental reason. There is some evidence that problems during pregnancy or childbirth may increase the risk of a child developing Tourette's syndrome. This may include problems such as prolonged labor, high levels of maternal stress in pregnancy, or babies with very low birth weight. On the other hand, the associated social isolation and the suppression of the symptoms by the TS child may make the tics even more severe, which would then be a non-developmental, secondary problem.

CONCLUSION

Our results indicate that the main effects of TS children were reflected by decreased FA values and increase RD values, which are sensitive measures of microstructural changes in both deep and superficial WM. Notably, the identified changes were not solely restricted to CSTC

circuit but also affected SWM within the primary motor and somatosensory cortex, commissural and association fibres and basal ganglia. These findings are interpreted as evidence for neuroplastic adaptation in TS. Also, it is worth mentioning that these results reflect early developmental structural changes in children patients with TS, which would likely differ from those that their symptom persist to adult with TS [Plessen et al., 2004]. Last, our findings suggest that combining atlas-based ROI analysis with TBSS was promising in depicting shared and unique microstructural abnormalities in early TS children depending on the used method, thereby a richer view of neural pathways involved in TS characterization was investigated.

REFERENCES

Ackermans L, Temel Y, Visser-Vandewalle V (2008): Deep brain stimulation in Tourette's syndrome. Neurotherapeutics 5:339–344.

Albin RL, Mink JW (2006): Recent advances in Tourette syndrome research. Trends Neurosci 29:175–182.

Alongi P, Iaccarino L, Perani D (2014): PET neuroimaging: Insights on Dystonia and Tourette syndrome and potential applications. Front Neurol 5:183

Bach M, Laun FB, Leemans A, Tax CM, Biessels GJ, Stieltjes B, Maier-Hein KH (2014): Methodological considerations on tract-based spatial statistics (TBSS). Neuroimage 100:358–369.

Basser PJ (1995): Inferring microstructural features and the physiological state of tissues from diffusion-weighted images. Nmr Biomed 8:333–344.

Basser PJ, Jones DK (2002): Diffusion-tensor MRI: Theory, experimental design and data analysis—A technical review. Nmr Biomed 15:456–467.

Basser PJ, Pierpaoli C (1996): Microstructural and physiological features of tissues elucidated by quantitative-diffusion-tensor MRI. J Magn Reson Ser B 111:209–219.

Basser PJ, Mattiello J, LeBihan D (1994): MR diffusion tensor spectroscopy and imaging. Biophys J 66:259–267.

Bigler ED, Mortensen S, Neeley ES, Ozonoff S, Krasny L, Johnson M, Lu J, Provencal SL, McMahon W, Lainhart JE (2007): Superior temporal gyrus, language function, and autism. Dev Neuropsychol 31:217–238.

Bohlhalter S, Goldfine A, Matteson S, Garraux G, Hanakawa T, Kansaku K, Wurzman R, Hallett M (2006): Neural correlates of tic generation in Tourette syndrome: An event-related functional MRI study. Brain 129:2029–2037.

Bronfeld M, Bar-Gad I (2013): Tic Disorders: What Happens in the Basal Ganglia? Neuroscientist 19:101–108.

Budde MD, Xie M, Cross AH, Song SK (2009): Axial diffusivity is the primary correlate of axonal injury in the experimental autoimmune encephalomyelitis spinal cord: A quantitative pixelwise analysis. J Neurosci 29:2805–2813.

Burgund ED, Kang HC, Kelly JE, Buckner RL, Snyder AZ, Petersen SE, Schlaggar BL (2002): The feasibility of a common stereotactic space for children and adults in fMRI studies of development. Neuroimage 17:184–200.

Cavanna AE, Stecco A, Rickards H, Servo S, Terazzi E, Peterson B, Robertson MM, Carriero A, Monaco F (2010): Corpus callosum abnormalities in Tourette syndrome: An MRI-DTI study of monozygotic twins. J Neurol Neurosurg Psychiatry 81:533–535.

Ceritoglu C, Oishi K, Li X, Chou MC, Younes L, Albert M, Lyketsos C, van Zijl PCM, Miller MI, Mori S (2009): Multi-contrast large deformation diffeomorphic metric mapping for diffusion tensor imaging. Neuroimage 47:618–627.

Cheng B, Braass H, Ganos C, Treszl A, Biermann-Ruben K, Hummel FC, Muller-Vahl K, Schnitzler A, Gerloff C, Munchau A, Thomalla G (2014): Altered intrahemispheric structural connectivity in Gilles de la Tourette syndrome. Neuroimage Clin 4:174–181.

Church JA, Fair DA, Dosenbach NUF, Cohen AL, Miezin FM, Petersen SE, Schlaggar BL (2009): Control networks in paediatric Tourette syndrome show immature and anomalous patterns of functional connectivity. Brain 132:225–238.

Comings DE, Comings BG, Devor EJ, Cloninger CR (1984): Detection of major gene for gilles-De-La-Tourette syndrome. Am J Hum Genet 36:586–600.

de Groot M, Vernooij MW, Klein S, Ikram MA, Vos FM, Smith SM, Niessen WJ, Andersson JL (2013): Improving alignment in Tract-based spatial statistics: Evaluation and optimization of image registration. Neuroimage 76:400–411.

Draganski B, Martino D, Cavanna AE, Hutton C, Orth M, Robertson MM, Critchley HD, Frackowiak RS (2010): Multispectral brain morphometry in Tourette syndrome persisting into adulthood. Brain 133:3661–3675.

Faria AV, Zhang JY, Oishi K, Li X, Jiang HY, Akhter K, Hermoye L, Lee SK, Hoon A, Stashinko E, Miller MI, van Zijl PCM, Mori S (2010): Atlas-based analysis of neurodevelopment from infancy to adulthood using diffusion tensor imaging and applications for automated abnormality detection. Neuroimage 52: 415–428.

Ganos C, Roessner V, Munchau A (2013): The functional anatomy of Gilles de la Tourette syndrome. Neurosci Biobehav Res 37: 1050–1062.

Gerard E, Peterson BS (2003): Developmental processes and brain imaging studies in Tourette syndrome. J Psychosom Res 55:13–22.

Haber SN, Knutson B (2010): The Reward Circuit: Linking Primate Anatomy and Human Imaging. Neuropsychopharmacol 35:4–26.

Harris K, Singer HS (2006): Tic disorders: Neural circuits, neurochemistry, and neuroimmunology. J Child Neurol 21:678–689.

Huppi PS, Dubois J (2006): Diffusion tensor imaging of brain development. Semin Fetal Neonatal Med 11:489–497.

Hyde TM, Stacey ME, Coppola R, Handel SF, Rickler KC, Weinberger DR (1995): Cerebral morphometric abnormalities in Tourette's syndrome: A quantitative MRI study of monozygotic twins. Neurology 45:1176–1182.

Jenkinson M, Beckmann CF, Behrens TE, Woolrich MW, Smith SM (2012): Fsl. Neuroimage 62:782–790.

Jeppesen SS, Debes NM, Simonsen HJ, Rostrup E, Larsson HB, Skov L (2014): Study of medication-free children with Tourette syndrome do not show imaging abnormalities. Movement Disord 29:1212–1216.

Kasahara K, Hashimoto K, Abo M, Senoo A (2012): Voxel- and atlas-based analysis of diffusion tensor imaging may reveal focal axonal injuries in mild traumatic brain injury - comparison with diffuse axonal injury. Magn Reson Imaging 30:496–505.

Leckman JF, Riddle MA, Hardin MT, Ort SI, Swartz KL, Stevenson J, Cohen DJ (1989): The Yale Global Tic Severity

Scale: Initial testing of a clinician-rated scale of tic severity. J Am Acad Child Adolesc Psychiatry 28:566–573.

Li XL, Sun JH, Li F, Huang MJ, Li QQ, Wu QZ, Zhang TJ, Guo LT, Gong QY, Huang XQ (2010): [Microstructural abnormalities of basal ganglia and thalamus in children with first-episode Tourette's syndrome: A diffusion tensor imaging study]. Sichuan Da Xue Xue Bao. Yi Xue Ban = Journal of Sichuan University. Medical Science Edition 41:284–287.

Liu Y, Miao W, Wang J, Gao P, Yin G, Zhang L, Lv C, Ji Z, Yu T, Sabel BA, He H, Peng Y (2013): Structural abnormalities in early Tourette syndrome children: A combined voxel-based morphometry and tract-based spatial statistics study. Plos One 8:e76105

Makki MI, Behen M, Bhatt A, Wilson B, Chugani HT (2008): Microstructural abnormalities of striatum and thalamus in children with Tourette syndrome. Movement Disorders: Official Journal of the Movement Disorder Society 23:2349–2356.

McNaught KS, Mink JW (2011): Advances in understanding and treatment of Tourette syndrome. Nat Rev Neurol 7:667–676.

Miller MI, Christensen GE, Amit Y, Grenander U (1993): Mathematical textbook of deformable neuroanatomies. Proc Natl Acad Sci U S A 90:11944–11948.

Miller M, Banerjee A, Christensen G, Joshi S, Khaneja N, Grenander U, Matejic L (1997): Statistical methods in computational anatomy. Stat Method Med Res 6:267–299.

Mink JW (2006): Neurobiology of basal ganglia and Tourette syndrome: Basal ganglia circuits and thalamocortical outputs. Adv Neurol 99:89–98.

Muller-Vahl KR, Grosskreutz J, Prell T, Kaufmann J, Bodammer N, Peschel T (2014): Tics are caused by alterations in prefrontal areas, thalamus and putamen, while changes in the cingulate gyrus reflect secondary compensatory mechanisms. BMC Neurosci 15:6.

Muller-Vahl KR, Kaufmann J, Grosskreutz J, Dengler R, Emrich HM, Peschel T (2009): Prefrontal and anterior cingulate cortex abnormalities in Tourette Syndrome: Evidence from voxel-based morphometry and magnetization transfer imaging. BMC Neurosci 10:47.

Nazeri A, Chakravarty MM, Felsky D, Lobaugh NJ, Rajji TK, Mulsant BH, Voineskos AN (2013): Alterations of superficial white matter in schizophrenia and relationship to cognitive performance. Neuropsychopharmacol 38:1954–1962.

Nichols TE, Holmes AP (2002): Nonparametric permutation tests for functional neuroimaging: A primer with examples. Hum Brain Mapp 15:1–25.

Oishi K, Faria A, Jiang HY, Li X, Akhter K, Zhang JY, Hsu JT, Miller MI, van Zijl PCM, Albert M, Lyketsos CG, Woods R, Toga AW, Pike GB, Rosa-Neto P, Evans A, Mazziotta J, Mori S (2009): Atlas-based whole brain white matter analysis using large deformation diffeomorphic metric mapping: Application to normal elderly and Alzheimer's disease participants. Neuroimage 46:486–499.

Perera H, Abayanayaka C (2012): Management of severe pediatric tourette syndrome resistant to drug treatment. Case Rep Psychiatry 2012:497160

Petek E, Windpassinger C, Vincent JB, Cheung J, Boright AP, Scherer SW, Kroisel PM, Wagner K (2001): Disruption of a novel gene (IMMP2L) by a breakpoint in 7q31 associated with Tourette syndrome. Am J Hum Genet 68:848–858.

Peterson BS, Staib L, Scahill L, Zhang HP, Anderson C, Leckman JF, Cohen DJ, Gore JC, Albert J, Webster R (2001): Regional brain and ventricular volumes in Tourette syndrome. Arch Gen Psychiatry 58:427–440.

Peterson BS, Thomas P, Kane MJ, Scahill L, Zhang H, Bronen R, King RA, Leckman JF, Staib L (2003): Basal Ganglia volumes in patients with Gilles de la Tourette syndrome. Arch Gen Psychiatry 60:415–424.

Plessen KJ, Wentzel-Larsen T, Hugdahl K, Feineigle P, Klein J, Staib LH, Leckman JF, Bansal R, Peterson BS (2004): Altered interhemispheric connectivity in individuals with Tourette's disorder. Am J Psychiatry 161:2028–2037.

Plessen KJ, Bansal R, Peterson BS (2009): Imaging evidence for anatomical disturbances and neuroplastic compensation in persons with Tourette syndrome. J Psychosom Res 67:559–573.

Pourfar M, Feigin A, Tang CC, Carbon-Correll M, Bussa M, Budman C, Dhawan V, Eidelberg D (2011): Abnormal metabolic brain networks in Tourette syndrome. Neurology 76:944–952.

Retz-Junginger P, Retz W, Blocher D, Stieglitz RD, Georg T, Supprian T, Wender PH, Rosler M (2003): [Reliability and validity of the Wender-Utah-Rating-Scale short form. Retrospective assessment of symptoms for attention deficit/hyperactivity disorder]. Der Nervenarzt 74:987–993.

Scahill L, Riddle MA, McSwiggin-Hardin M, Ort SI, King RA, Goodman WK, Cicchetti D, Leckman JF (1997): Children's Yale-brown obsessive compulsive scale: Reliability and validity. J Am Acad Child Adolesc Psychiatry 36:844–852.

Shiva K, Ryan NS, Malone IB, Marc M, David C, Ridgway GR, Hui Z, Fox NC, Sebastien O (2012): The importance of group-wise registration in tract based spatial statistics study of neurodegeneration: A simulation study in Alzheimer's disease. Plos One 7:e45996–e45996

Singer HS (2005): Tourette's syndrome: From behaviour to biology. Lancet Neurol 4:149–159.

Singer HS, Minzer K (2003): Neurobiology of Tourette's syndrome: Concepts of neuroanatomic localization and neurochemical abnormalities. Brain Dev-Jpn 25:S70–S84.

Smith SM, Nichols TE (2009): Threshold-free cluster enhancement: Addressing problems of smoothing, threshold dependence and localisation in cluster inference. Neuroimage 44:83–98.

Smith SM, Jenkinson M, Johansen-Berg H, Rueckert D, Nichols TE, Mackay CE, Watkins KE, Ciccarelli O, Cader MZ, Matthews PM, Behrens TE (2006): Tract-based spatial statistics: Voxelwise analysis of multi-subject diffusion data. Neuroimage 31:1487–1505.

Song SK, Sun SW, Ju WK, Lin SJ, Cross AH, Neufeld AH (2003): Diffusion tensor imaging detects and differentiates axon and myelin degeneration in mouse optic nerve after retinal ischemia. Neuroimage 20:1714–1722.

Song SK, Yoshino J, Le TQ, Lin SJ, Sun SW, Cross AH, Armstrong RC (2005): Demyelination increases radial diffusivity in corpus callosum of mouse brain. Neuroimage 26:132–140.

Sowell ER, Kan E, Yoshii J, Thompson PM, Bansal R, Xu DR, Toga AW, Peterson BS (2008): Thinning of sensorimotor cortices in children with Tourette syndrome. Nat Neurosci 11:637–639.

Stern E, Silbersweig DA, Chee KY, Holmes A, Robertson MM, Trimble M, Frith CD, Frackowiak RSJ, Dolan RJ (2000): A functional neuroanatomy of ties in Tourette syndrome. Arch Gen Psychiatry 57:741–748.

Stokes A, Bawden HN, Camfield PR, Backman JE, Dooley JM (1991): Peer problems in Tourettes disorder. Pediatrics 87: 936–942.

Thomalla G, Siebner HR, Jonas M, Baumer T, Biermann-Ruben K, Hummel F, Gerloff C, Muller-Vahl K, Schnitzler A, Orth M, Munchau A (2009): Structural changes in the somatosensory

system correlate with tic severity in Gilles de la Tourette syndrome. Brain 132:765–777.

Tyszka JM, Readhead C, Bearer EL, Pautler RG, Jacobs RE (2006): Statistical diffusion tensor histology reveals regional dysmyelination effects in the shiverer mouse mutant. Neuroimage 29:1058–1065.

Worbe Y, Malherbe C, Hartmann A, Pelegrini-Issac M, Messe A, Vidailhet M, Lehericy S, Benali H (2012): Functional immaturity of cortico-basal ganglia networks in Gilles de la Tourette syndrome. Brain 135:1937–1946.

Worbe Y, Marrakchi-Kacem L, Lecomte S, Valabregue R, Poupon F, Guevara P, Tucholka A, Mangin JF, Vidailhet M, Lehericy S, Hartmann A, Poupon C (2015): Altered structural connectivity of cortico-striato-pallido-thalamic networks in Gilles de la Tourette syndrome. Brain 138:472–482.